Study of a Miniaturized Cylindrical Shaped Antenna Resonating at 6.5 GHz Frequency for 6 GHz Band Wi−Fi Routers

Md. Ershadul Haque, Tanvir Hossain, Sami Ul Hoque, Salah Uddin, Manoranjan Paul

Abstract – **The Federal Communications Commission (FCC) has adopted a new rule, on April 23, 2020, making 1200 Megahertz of frequency spectrum in wireless fidelity (Wi−Fi) 6 GHz frequency band (5.925−7.125) GHz for the unlicensed user. Based on the announcement, a cylindrical shaped antenna resonated at 6.5 GHz frequency is proposed for Wi−Fi applications in the routers through this work. A material named FR4−Epoxy having dielectric constant 4.4 and loss tangent 0.02 is used in substrate layer that builds up the antenna compact enough. The antenna with a dimension of length 60 mm and radius 3.55 mm at all is manifested in a tiny cylindrical shape and consequently, can be a compatible candidate for implementation in wireless routers conveniently. The behaviour of radiation characteristics of cylindrical shaped antenna is analyzed. Circular polarization of radiation surrounding the antenna, a very significant characteristic of an antenna to be applied for Wi−Fi applications, is realized by the proposed antenna. The value of gain, wide bandwidth cohering across the frequency band, minimum value of reflection coefficient and voltage standing wave ratio, high radiation efficiency, and all the other better performances pledge that the antenna is apposite to the Wi−Fi applications.**

Keywords – **Wi−Fi, Wireless router, Cylindrical shaped antenna, 6 GHz band.**

I. INTRODUCTION

Wireless fidelity (Wi−Fi) is a protocol of wireless communication systems. In the past decade, this protocol has found application in numerous wireless communication devices. Nowadays, Wi−Fi might be found in homes, offices, hospitals, educational institutions, parliament buildings, business institutions, airports, restaurants, and all over the place in our daily life. Many cities around the world have successfully established Wi−Fi networks covering the entire city.

Several frequency bands have been adopted for the Wi−Fi protocol. Conventionally, 2.4 GHz and 5 GHz frequency bands are deployed in most of the devices [1]. A Wi−Fi system developed by the equipment having better performances, i.e. antenna, microcontroller, converter, electronics circuits, etc. is capable of transmitting data at a high rate speed of up to 54 Mbps and beyond. A wireless router is the most preferable device to connect a client device at a distance which transmits data through an antenna. Wi−Fi antennas have many access points covering a territory known as hotspot. The hotspot should have a large extended range of up to about 100 metres [2]. In addition, the Wi−Fi protocol is incorporated into many other devices, such as laptop computers, desktop computers, smartphones, printers, and so on. Various sized and shaped antennas are used in the devices for the sake of having size and shape constraint. An antenna to be used in Wi−Fi application has to be considered according to some radiation characteristics. Wi−Fi network providing devices, namely routers and other battery driven devices have to count a good amount of loss for poor radiation characteristic of antenna [3]. A lot of study related to the antenna installed for the Wi−Fi applications is traced in the literature and discussed in following Section 2. Recently, The Federal Communications Commission (FCC) adopted a new frequency band where 1200 MHz spectrum from 5.925 GHz to 7.125 GHz is available for the unlicensed users on April 23, 2020 [4]. This new frequency band will increase the amount of channels and improve connectivity. This new frequency band will usher in the next generation Wi−Fi network and pays an important preface for the advance of Internet of Things (IoT). It will promote the rate of data transmission more than two and a half times faster than the present grade. Unlicensed devices are able to share the band with incumbent licensed service under the rule crafted to protect licensed service and enable both licensed and unlicensed operation.

The contributions of this work are to:

1. propose a miniaturized cylindrical shaped Wi−Fi antenna at the recently announced Wi−Fi 6 GHz frequency band by FCC to implement into the routers.
2. analyze the radiation characteristics of a cylindrical shaped antenna through its structural features so that can be assessed how efficiently it provides a Wi−Fi network.
3. develop 89% radiation efficiency that is most significant and desirable attribute of Wi−Fi antenna for application into the routers and battery driven devices.
4. establish the major lobe of radiation pattern circularly around the antenna and to avoid the minor lobe which is toward vertical direction from the antenna.

Article history: Received February 16, 2021; Accepted December 16, 2021

Md. Ershadul Haque, Tanvir Hossain, Sami Ul Hoque and Salah Uddin are with the Department of EEE, Feni University, Feni-3900, Bangladesh, E-mails: chairmaneeedept@feniuniversity.edu.bd; tanvirhossainzillu@gmail.com; samiul@feniuniversity.edu.bd; salahuddin@feniuniversity.edu.bd

Manoranjan Paul is with School of Computing & Mathematics, Charles Sturt University, Bathurst, NSW, Australia, E-mail: mpaul@csu.edu.au

The paper is organized as follows: Section 2 discusses related work. The architecture of the proposed cylindrical shape model is presented in Section 3. Section 4 includes the mathematical model of the antenna. Section 5 explains the computational results and discussion. The conclusion is drawn in Section 6.

II. RELATED WORK

The paper [5] evolves a 2.4 GHz microstrip antenna for implementation of Wi−Fi network by applying the differential evolution (DE) method. The size of the antenna structure was $50 \times 50 \times 1.6\ \text{mm}^3$. A constrained optimization problem was derived. The DE algorithm satisfies the requirements of the designing scenario. The antenna can be used into the routers as well as personal computers within an indoor circumstance. A dual band multiple input multiple output (MIMO) antenna has been proposed for the Wi−Fi and WiMax applications [6]. The antenna is composed of two sickle shaped patches, microstrip feed line, and rectangular shaped slot on ground plane. The results refer that the presented antenna has a better operating bandwidth at over −10 dB reflection coefficient. [7] presents a wide band antenna array for Wi−Fi. A linear phased array antenna designed with beam steering capability [8] is demonstrated to use for Wi−Fi and long−term evolution (LTE) portable standard applications. The antenna, using the radiating elements in array, performs dual frequency operation cohering two frequency band (2.35−2.8) GHz and (5−5.5) GHz. FR4 material was deployed for the substrate of the antenna. The represented antenna is able to be used for a portable and small base station. Design of a printed doubled sided dipole antenna to be implemented for providing Wi−Fi network within 2.4 GHz and 5.2 GHz frequency bands was proposed in [9]. The proposed dipole antenna can be considered as appropriate to integrate into monolithic microwave integrated circuit (MMIC) devices. An antenna consisting of a L−shaped radiator for Wi−Fi application has been presented in [10]. [11] is discussed with the introducing a 2.4 GHz dipole antenna. A study on the behaviour of the proposed dipole antenna with baluns before the conversion of its structure from wire to printed configuration was also presented. The antenna with integrated via−hole balun printed on FR4, Rogers TMM 4, and Rogers RT6002 substrates are shown. An investigation of the performance of a rectangular spiral configured microstrip patch antenna integrated with light emitting diode (LED) for Wi−Fi network implementation was presented in [12]. The antenna was intended to operate at 2.4 GHz frequency. The placement of LED into the spiral pattern is optimized through genetic algorithm (GA) technique. Measured performance of the antenna is evaluated in terms of return loss, gain, and radiation pattern. The presented antenna was fabricated on FR4 substrate. A tapered meandered bowtie shaped dual band operating at 2.4 GHz and 5.8 GHz antenna was proposed for Wi−Fi applications [13]. It is printed on FR4 substrate and the entire volume of the antenna is $21.5 \times 15 \times 1.6\ \text{mm}^3$. A textile based wearable, dual band MIMO quad mode substrate integrated wave guide antenna was introduced in [14]. The proposed antenna covers Bluetooth, Wi−Fi 2.4GHz and 5.2GHz and 5.8GHz frequency bands. It has an overall size of $115 \times 122 \times 4.1\text{mm}^3$. A dual band planar monopole antenna fed by 'coplanar waveguide' to implement for Wi−Fi and 4G (LTE) operating frequency was demonstrated in [15]. A small size of $41.6 \times 28.38 \times 1.52\ \text{mm}^3$ is occupied by the proposed antenna. Two frequency bands existing at (2.3−3.0) GHz and (4.7−5.9) GHz were obtained by optimization of the location and shape of the smiling slot. In [16], a printed diversity monopole antenna has been proposed to be used for Wi−Fi/WiMAX application. The antenna is comprised of two crescent shaped radiators installed symmetrically with respect to a defected ground plane and a neutralization line connects them. As a result, the antenna achieved better impedance matching and low mutual coupling. The computed and measured gain, radiation patterns, and other performances appreciate that the antenna can be chosen to be an appropriate candidate for MIMO portable device. A dual band Wi−Fi antenna designed using GA was proposed in [17]. The method states that at first the surface of the patch is divided into many pixels and then, a number of pixels are cut step by step. Thus, the desired antenna was evaluated. Authors of [18] introduced an E−shaped patch and dual band antenna for Wi−Fi and WiMAX applications. The proposed methodology includes cavity model analysis where a slotted set up is considered to be a perturbed cavity for characterizing the resonant frequency of the respective modes. A model of equivalent circuit is also presented in the paper based on the coupled resonator theories to analyze the behaviour of the antenna. In [19], a dual band microstrip patch antenna design was proposed for WiMax and Wi−Fi applications. In the design of the antenna, a C slot structure and two parallel slit have been localized on patch and ground, respectively. The authors represented a dual frequency rectangular microstrip patch antenna for Wi−Fi and WiMAX supporting wireless application [20]. A pair of symmetrical U shaped slot is placed in the patch to obtain dual band operations. A physical approach is followed to derive an expression for resonant frequencies by surface current distribution analysis of the patch. The parametric study of slot demonstrates that the geometry of antenna can be applied to different standards by varying the parameters of slots properly.

III. ARCHITECTURE OF THE PROPOSED DESIGN

A miniaturized cylindrical antenna is designed to resonate within the Wi−Fi 6 GHz frequency band (5.925−7.125) GHz so that can easily be implemented into a wireless router.

The antenna is simulated with ANSYS high−frequency structure simulator (HFSS^{TM}), Ver. 15.0, software, an three dimensional electromagnetic simulation tool for designing and simulating high−frequency electronic products, such as antennas, antenna arrays, RF or microwave components, high−speed interconnects, filters, connectors, IC packages, and printed circuit boards. Engineers worldwide use it to design high−frequency, high−speed electronics found in communications systems, advanced driver assistance systems (ADAS), satellites, and internet of things (IoT) products [21].

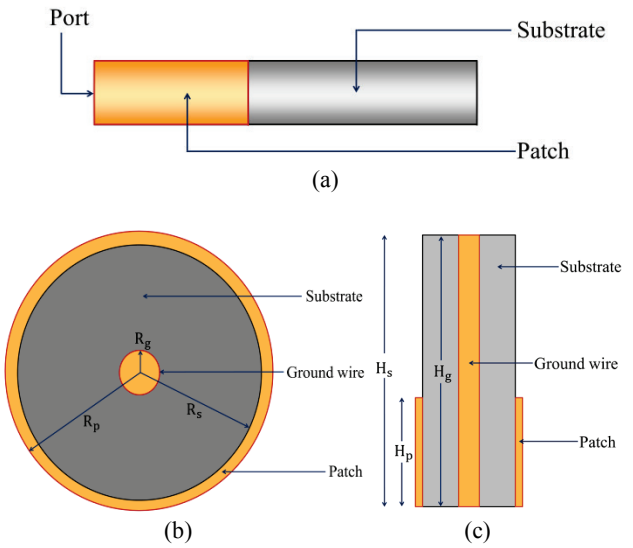

Fig. 1. Schematic representation of the proposed antenna: (a) Front view, (b) Horizontal cross section view and (c) Vertical cross section view.

It has been stimulated to acquire the aimed resonant frequency by applying some modification operation on the materials such as the radiating element, substrate, and ground. The resonant frequency of an antenna is correlated with the structural feature of its elements. The following formula, feasible to determine the resonant frequency of the antenna, is given by, [22]

$$f_{mn} = \frac{c}{2\sqrt{\varepsilon_r}}\sqrt{\left[\left(\frac{m}{2R\emptyset_e}\right)^2 + \left(\frac{n}{z_e}\right)^2\right]} \qquad (1)$$

where $2R\emptyset_e = 2R\emptyset_0 + h/\sqrt{\varepsilon_r}$ is the effective circumferential length of the patch and $Z_e = Z_m + h/\sqrt{\varepsilon_r}$ is the effective axial length. The actual dimensions of the patch are Z_m and $2R\emptyset_0$. R is the cylinder radius, $\emptyset_0$ is azimuthal angle, h is the substrate height, ε_r is the dielectric constant of the substrate, and mn is the mode number.

The antenna is consisted of three cylindrical layers, such as, a hollow cylindrical substrate layer, a hollow cylindrical patch layer, and a cylindrical ground wire as shown in Fig. 1. Fig. 1(a) illustrates the schematic representation of the proposed antenna in the prospect of front view, Fig. 1(b) depicts the horizontal cross section view along xy−plane, and Fig. 1(c) presents the vertical cross section view along yz−plane or xz−plane. Now, let us encounter the dimension of the antenna. It has a cylindrical ground wire of 60 mm length designated as H_g along z−axis and a uniform radius of 0.5 mm designated as R_g along xy−plane. A hollow cylindrical substrate layer is mounted around the ground wire. It is also 60 mm long designated as H_s along z−axis and has a uniform radius of 3.5 mm from the centre of the ground wire to the outer surface of the substrate layer as designated by R_s along xy−plane. Hence, the thickness of the hollow cylindrical substrate layer stands at 3 mm. A sample of FR4−Epoxy material is deployed to be the substrate material. It has a dielectric constant of 4.4 and a loss tangent ($tan\delta$) of 0.02. The hollow cylindrical patch layer is mounted around the substrate layer. The length of the hollow cylinder of patch layer designated as H_p is 18 mm along Z−axis. The uniform radius along xy−plane from the centre of the ground wire to the outer surface of patch layer is 3.55 mm as designated with R_p. Therefore, the hollow cylindrical patch layer has 0.05 mm thickness. Also, copper is used for the ground wire and the patch layer. The antenna has been excited by a 50 Ω lumped port.

TABLE I
DESIGN VALUES OF THE MATERIALS

Length		Radius	
Parameters	Values (mm)	Parameters	Values (mm)
H_p	18	R_p	3.55
H_s	60	R_s	3.5
H_g	60	R_g	0.5

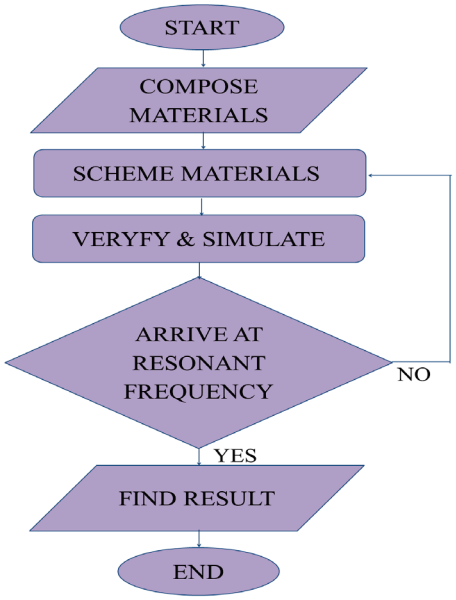

Fig. 2. Flow chart to explain the methodology of developing the antenna.

Table I summarizes the dimensions of employed materials of the proposed antenna using the related parameters shown in Fig. 1.

The flow chart given in Fig. 2 might reveal the methodology of the developed antenna. The methodology is initiated over the picking out the respective materials of the antenna elements. Then, the materials are fetched to the actual shape found according to the modelling mathematical resolutions. After that, the antenna is checked for either the resonant frequency is achieved at the expected frequency or not. If it is true, the strategies proceed ahead otherwise regressed on the forming of the material phase. The steps are finalized through the evaluation of all the results.

IV. MATHEMATICAL MODEL

A. Cavity Analysis

To model the patch, consider two axial as well as two circumferential slots. Solution to the boundary value problems inside the cavity including feed to be the source may provide the distribution of field in the slots. The solutions are represented by several modes which produce a set of distributions of field in the side walls. These sets of distributions of field are utilized as the source of radiations.

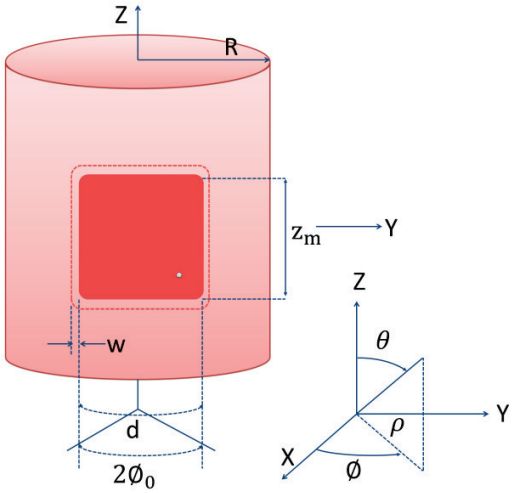

Fig. 3. A patch on the surface of a cylindrical substrate material.

A.1. Internal Field

Consider the rectangular patch seen by Fig. 3. If the substrate material is assumed very thin, then, the E−field has only the ρ −component. Following equations can be expressed in the case of E−field and H−field using the planer case [23], [24],

$$E_\rho(\emptyset,z) = = jI_0Z_0k\sum_{p=0}^{\infty}\sum_{q=0}^{\infty}\frac{\varphi_{pq}(\emptyset,z)\varphi_{pq}(\emptyset_f,z_f)}{k^2-k_{pq}^2}G_{pq} \quad (2)$$

$$H_\emptyset(\emptyset,z) = -I_0\sum_{p=0}^{\infty}\sum_{q=0}^{\infty}\frac{\varphi_{pq}(\emptyset,z)\varphi_{pq}(\emptyset_f,z_f)}{k^2-k_{pq}^2} \times tan\left(\frac{q\pi z}{z_m}\right)\frac{q\pi}{z_m}G_{pq} \quad (3.a)$$

$$H_z(\emptyset,z) = = -I_0\sum_{p=0}^{\infty}\sum_{q=0}^{\infty}\frac{\varphi_{pq}(\emptyset,z)\varphi_{pq}(\emptyset_f,z_f)}{k^2-k_{pq}^2} \times tan\left(\frac{p\pi\emptyset}{2\emptyset_0}\right)\frac{p\pi}{2R\emptyset_0}G_{pq} \quad (3.b)$$

Here,

$$k_{pq}^2 = \left(\frac{p\pi}{2R\emptyset_0}\right)^2+\left(\frac{q\pi}{z_m}\right)^2 \quad (4)$$

$$k^2 = \varepsilon_r\left(1-j\delta_{eff}\right)k_0^2 \quad (5)$$

$$\varphi_{pq}(\emptyset,z) = \sqrt{\frac{\varepsilon_{0p}\varepsilon_{0q}}{z_m d}}cos\left(\frac{p\pi\emptyset}{2\emptyset_0}\right)cos\left(\frac{q\pi z}{z_m}\right) \quad (6)$$

$$\varepsilon_{0k} = \begin{Bmatrix}1 & k=0\\ 2 & k\neq 0\end{Bmatrix} \quad (7)$$

$$G_{pq} = sinc\left(\frac{p\pi\Delta_\emptyset}{2d}\right)sinc\left(\frac{q\pi\Delta_z}{2z_m}\right) \quad (8)$$

p, q are the numbers of the modes. $k_0 = 2\pi/\lambda_0$. Dielectric constant of the substrate material is ε_r. $\emptyset_f$, z_f is the location of feed, $\Delta_\emptyset$, Δ_z are the extensions of probe in $\emptyset$ and z, respectively for a rectangular probe. $\emptyset_0 = d/2R$, z_m, d, and R are conferred as Fig. 3. δ_{eff} is the effective loss tangent, includes all the losses of the cavity.

A.2. External Field

E−field into the walls of the cavity may be represented through the equivalent magnetic currents $M_\emptyset$ and M_z [25]. The fields can be found through two orthogonal components of vector potential. The components are intended to be, for instant, A_z and F_z. A designates the magnetic vector potential, on the other hand, F designates the electric vector potential. Expanding of both field and radiated field in the slot and outside the cylinder, respectively within cylindrical mode gives rise to the equations of axial component of the vector potential. The conditions of radiation at infinity dictate the second kind Hankel function employed utilized for time dependent term $\varepsilon^{j\omega t}$. Using asymptotic formulas for near/far – field transformations, for $A_\theta = -A_Z sin\theta$ and $F_\theta = -F_z sin\theta$ in far-field, the equations are determined as follow [26],

$$A_\theta = \frac{\exp(-jk_0r)}{k_0\pi r\eta}\sum_{n=-\infty}^{\infty}e^{jn\emptyset}j^n\frac{\tilde{E}_z^s(n,k_0cos\theta)}{H_n^{(2)}(k_0Rsin\theta)sin\theta} \quad (9.a)$$

$$F_\theta = = \frac{\exp(-jk_0r)}{k_0\pi r}\sum_{n=-\infty}^{\infty}e^{jn\emptyset}j^{n+1}\left[\frac{cos\theta n\tilde{E}_z^s(n,k_0cos\theta)}{k_0Rsin^2\theta H_n^{(2)'}(k_0Rsin\theta)} - \frac{\tilde{E}_\emptyset^s(n,k_0cos\theta)}{H_n^{(2)'}(k_0Rsin\theta)}\right] \quad (9.b)$$

Here, $\tilde{E}_z^s(n,k_z)$ and $\tilde{E}_\emptyset^s(n,k_z)$ are Fourier transformations of slot fields $E_z^s(\emptyset)$ and $E_\emptyset^s(z)$, respectively. $H_n^{(2)}(z)$ is second kind and n^{th} order Hankel function and $H_n^{(2)'}(z)$ is derivative of that Hankel function. Then, from far−field approximation, the radiated electric field and magnetic field are,

$$E_\theta = \eta H_\emptyset = -j\omega\mu A_\theta \quad (10.a)$$

$$E_\emptyset = \eta H_\theta = jk_0F_\theta \quad (10.b)$$

where η is called free space impedances. Now, the far−field radiation in the axial slots from each mode will be,

$$E_{\emptyset,q}(r,\emptyset,\theta) = = V_{pq}\frac{\exp(-jk_0r)}{2\pi^2rR}\frac{k_0cos\theta[\exp(jk_0z_mcos\theta)\cos(q\pi)-1]}{\left(\frac{q\pi}{z_m}\right)^2-k_0^2\cos^2\theta} \times e^{-jk_0cos\theta z_m/2}\sum_{n=0}^{\infty}\frac{\varepsilon_n j^{n+1}\cos[n(\emptyset\pm\emptyset_0)]}{H_n^{(2)'}(k_0Rsin\theta)} \times sinc\left(\frac{nw}{2R}\right)\begin{bmatrix}1\\-\cos(p\pi)\end{bmatrix} \quad (11)$$

Upper term in the bracket is implemented for the slot position at $\emptyset = -\emptyset_0$, the lower term into the bracket is implemented for the slot position at $\emptyset = +\emptyset_0$, and $-z_m/2 \le z \le z_m/2$.

$$\varepsilon_n = \begin{cases} 1 & n = 0 \\ 2 & n > 0 \end{cases} \quad (12)$$

The components of E−field in the case of circumferential slot for each p and q are,

$$E_{\theta,p}(r,\emptyset,\theta) = \\ = V_{pq}\frac{\exp(-jk_0r)}{2\pi^2 r} sinc\left(\frac{k_0 w}{2}cos\theta\right)\begin{bmatrix} -e^{-jk_0 cos\theta z_m/2} \\ \cos(\pi q)\, e^{jk_0 cos\theta z_m/2}\end{bmatrix} \\ \times \sum_{n=-\infty}^{\infty}\frac{[\cos(p\pi)\exp(-jn2\emptyset_0)-1]}{H_n^{(2)}(k_0 R sin\theta)sin\theta} \\ \times \frac{nj^n \exp[jn(\emptyset+\emptyset_0)]}{[\pi p/2\emptyset_0]^2 - n^2} \quad (13.a)$$

$$E_{\emptyset,p}(r,\emptyset,\theta) = \\ = \frac{V_{pq}}{k_0 R}\frac{\exp(-jk_0r)}{2\pi^2 r} sinc\left(\frac{k_0 w}{2}cos\theta\right)\begin{bmatrix} e^{-jk_0 cos\theta z_m/2} \\ -\cos(\pi q)\, e^{jk_0 cos\theta z_m/2}\end{bmatrix} \\ \times cot\theta \sum_{n=-\infty}^{\infty}\frac{[\cos(p\pi)\exp(-jn2\emptyset_0)-1]}{H_n^{(2)'}(k_0 R sin\theta)sin\theta} \\ \times \frac{n^2 j^{n+1}\exp[jn(\emptyset+\emptyset_0)]}{[\,\pi p/2\emptyset_0]^2 - n^2} \quad (13.b)$$

The upper term in the bracket is implemented for the slot position at $z = +z_d/2$, the lower term into the bracket is implemented for the slot position at $z = -z_d/2$, and $-\emptyset_0 \le \emptyset \le \emptyset_0$.

B. Surface Current Analysis

Consider a cylinder coated by substrate material has infinite length. The patch is presented in the manner of axial and circumferential surface current. The free space field in outward directions, field in substrate, and the current of patch are evaluated in the cylindrical mode. The tangential H-field on the patch metal can be given using the mode of the cavity model described in previous subsection. If the metal is taken into account as infinite thin, a relation between the surface current and the internal field of the cavity is found [25], [27].

Following equation represent the relation between internal H−field and surface current,

$$J^s = \hat{n} \times H \quad (14)$$

The current densities in patch are,

$$J^s_{z,pq} = H_{\emptyset,pq}(\emptyset,z) = -I_{pq}\sin\left(\frac{q\pi z}{z_m}\right)cos\left(\frac{p\pi\emptyset}{2\emptyset_0}\right) \quad (15.a)$$

$$J^s_{\emptyset,pq} = -H_{z,pq}(\emptyset,z) = I_{pq}\cos\left(\frac{q\pi z}{z_m}\right)sin\left(\frac{p\pi\emptyset}{2\emptyset_0}\right) \quad (15.b)$$

$$0 \le z \le z_m; 0 \le \emptyset \le \frac{d}{b} = 2\emptyset_0; p = 0,1,2,\dots; q = 0,1,2,\dots$$

b is the radius of the cylinder included substrate material. The far field radiation far is given by,

$$E_\theta(r,\emptyset,\theta) = \\ = -\omega\mu\frac{\exp(-jk_0r)}{\pi r} sin\theta \sum_{n=-\infty}^{\infty} j^n e^{jn\emptyset} C_m(n, k_0 cos\theta) \quad (16.a)$$

$$E_\emptyset(r,\emptyset,\theta) = \\ = k_0\frac{\exp(-jk_0r)}{\pi r} sin\theta \sum_{n=-\infty}^{\infty} j^n e^{jn\emptyset} C_e(n, k_0 cos\theta) \quad (16.b)$$

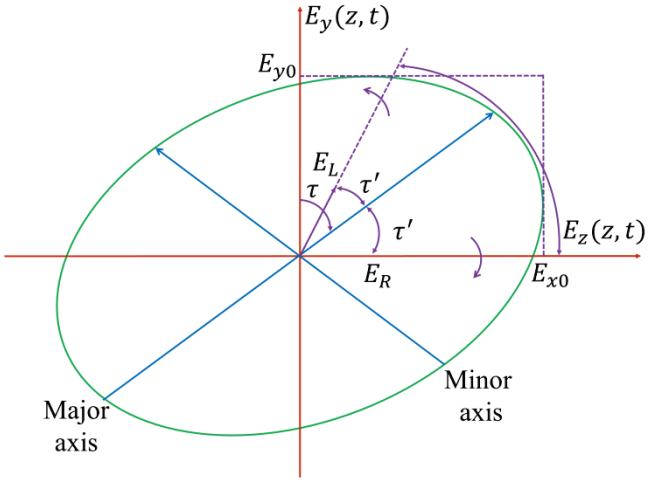

Fig. 4 The polarization ellipse at $z = 0$ to be function of time after a plane electromagnetic being rotated.

$$H_\theta = -\frac{E_\emptyset}{\eta} \quad (16.c)$$

$$H_\emptyset = \frac{E_\theta}{\eta} \quad (16.d)$$

where,

$$\begin{bmatrix} C_m \\ C_e \end{bmatrix} = M^{-1}\begin{bmatrix} J_z^s \\ J_\emptyset^s \end{bmatrix} = \frac{1}{\mathrm{DET}(M)}\begin{bmatrix} M_{22} & -M_{12} \\ -M_{21} & M_{11}\end{bmatrix}\begin{bmatrix} J_z^s \\ J_\emptyset^s \end{bmatrix} \quad (17)$$

J_z^s and $J_\emptyset^s$ are Fourier transformed current of the z–direction and $\emptyset$–direction, respectively. The details in regard to the elements of M−matrix can be seen by Ashkenazy et al. [27].

C. Boundary Condition

HFSS, indeed, makes use of a numerical procedure mentioned finite element method (FEM). It is a technique which subdivides a structure into multiple tiny subsections known as finite element. Solutions are obtained for the fields within the finite elements and the fields become interrelated, satisfying Maxwell's equations across inter-element boundaries [28].

A radiation boundary is utilized, allowing the electromagnetic waves to propagate on infinite condition far into the medium and let the electromagnetic waves be absorbed.

Radiation boundaries ought to be applied to the outer faces of the models. These faces have to remain at least a quarter wavelengths aloof from the surface of the radiator.

At the superficial edge of the radiation boundary, the 2nd–order boundary condition raises to the consideration. It is given by [28],

$$(\nabla \times E)_{tan} = jk_0 E_{tan} - \frac{f}{k_0}\nabla_{tan} \times (\nabla_{tan} \times E_{tan}) \\ + \frac{j}{k_0}\nabla_{tan}(\nabla_{tan}.E_{tan}) \quad (18)$$

where, E_{tan} is the component of E-field, tangential to the surface, k_0 is free space phase constant, corresponds to $\omega\sqrt{\mu_0\varepsilon_0}$.

D. Polarization

Polarization of the radiated waves can be regarded to be defined as the property of the electromagnetic waves that describes the time−varying direction and relative magnitude of the electric field vectors. In particular, Fig. 4 traced is a function of time by the vector's extreme point at a static position in space. The sense, in which it is observed, is along the direction of propagation.

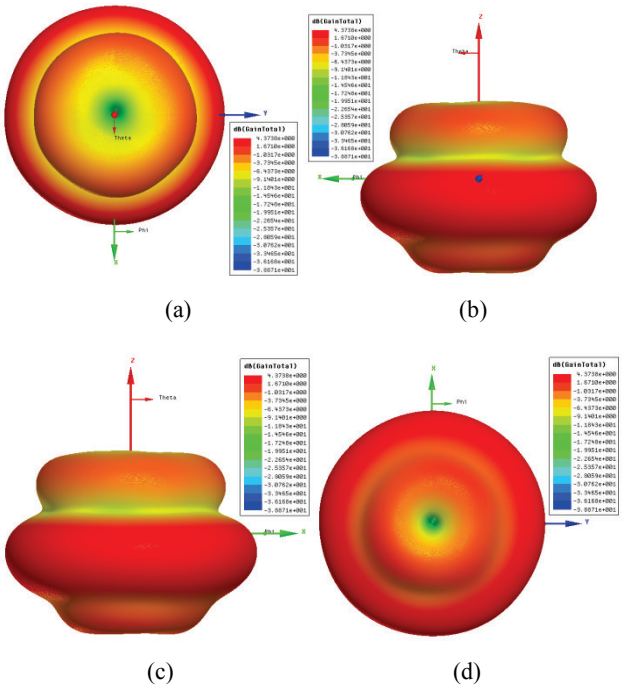

(a) (b) (c) (d)

Fig. 5. Gain of the antenna in the prospect of three dimensional radiation pattern: (a) Top side view, (b) Front side view, (c) Back side view, and (d) Bottom side view.

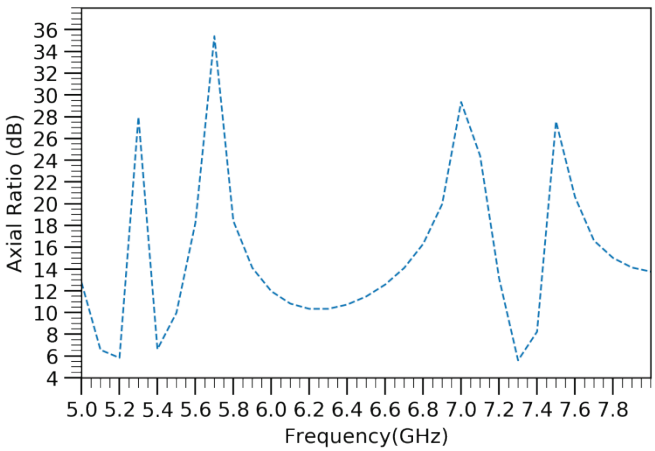

Fig. 6. Axial ratios in accordance with the related frequency steps.

The instantaneous field of a plane wave, travelling in the negative z direction as manifested in Fig. 4, may be given by, [29]

$$E(z,t) = \hat{a}_x E_x(z,t) + \hat{a}_y E_y(z,t) \tag{19}$$

The instantaneous components are related to their complex counterparts as,

$$E_x(z,t) = Re\left[E_{x0}e^{j(\omega t+kz+\emptyset_x)}\right] = E_{x0}\cos(\omega t + kz + \emptyset_x) \tag{20}$$

and

$$E_y(z,t) = Re\left[E_{y0}e^{j(\omega t+kz+\emptyset_y)}\right] = E_{y0}\cos\left(\omega t + kz + \emptyset_y\right) \tag{21}$$

Here, E_{x0} and E_{y0} are maximum magnitude of the x and y components, respectively.

Circular polarization can be obtained once the magnitude of the two components become similar and the phase difference with respect to time between two element is odd multiples of $\pi/2$. Consequently, [30]

$$|E_x| = |E_y| \Rightarrow E_{x0} = E_{y0} \tag{22}$$

For clockwise,

$$\Delta\emptyset = \emptyset_y - \emptyset_x = +\left(\frac{1}{2} + 2n\right)\pi; \quad n = 0,1,2,\ldots, \tag{23}$$

For counter−clockwise,

$$\Delta\emptyset = \emptyset_y - \emptyset_x = -\left(\frac{1}{2} + 2n\right)\pi, \quad n = 0,1,2,\ldots, \tag{24}$$

In the case of wave propagation is reversed, i.e. positive z direction, the phase Eqs. (23) and (24) must be interchanged for clockwise and counter−clockwise rotations.

V. Result and Discussion

The proposed antenna has appeared before in a slender cylindrical shape. Already depicted in Section 3, the length and radius of the entire antenna is raised to 60 mm and 3.55 mm, respectively. The performance of the antenna is appraised in an air medium. The resonant frequency of the antenna is accomplished at 6.5 GHz. The maximum value of gain G is attained 4.37 dB. It can be expressed by $G = \eta_{rad}D$, where η_{rad} is the radiation efficiency and D is the directivity described below in this section. Fig. 5 illustrates the maximum gain including three dimensional radiation pattern. The radiation pattern is evaluated in the far-field scenario. The figure narrates that the major lobe defined by the radiation lobe which contains the direction of maximum radiation is found approximately at the θ direction from 30^o to 330^o and the ϕ direction from 0^o to 360^o. Minor lobes usually represent the radiation at undesired directions. It should be minimized as possible and is seen rarely in the radiation pattern of the proposed antenna. Axial ratio γ, a ratio between the major and the minor axis of a circularly polarised radiation pattern, meets a value of 11.47 dB. The affair gets encountered while having a glance over the Fig. 6. The equation, $\gamma = \frac{Major\ axis}{Minor\ axis}$, yields a formulation of the axial ratio. The antenna has the minimum value of reflection coefficient −49.5 dB at resonant frequency as seen in Fig. 7. It has more than 600 MHz or 9.2% wide bandwidth at −10 dB reflection coefficient revealed from that figure. Relative

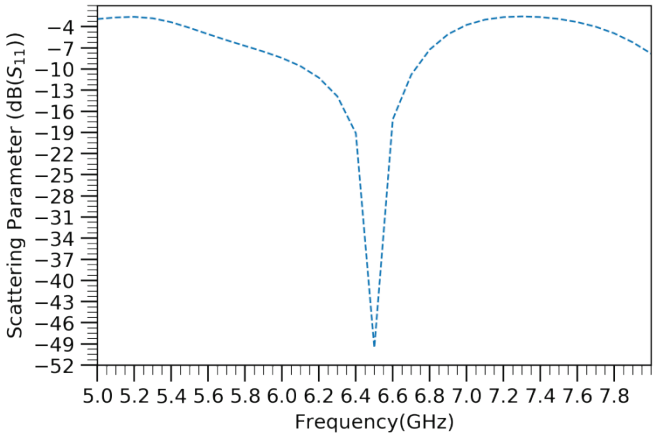

Fig. 7. Reflection coefficients of the antenna following the frequencies.

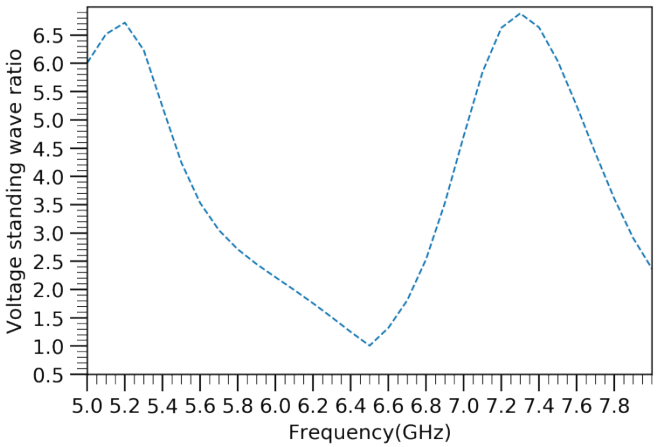

Fig. 8. Voltage standing wave ratios of the antenna and the corresponding frequencies.

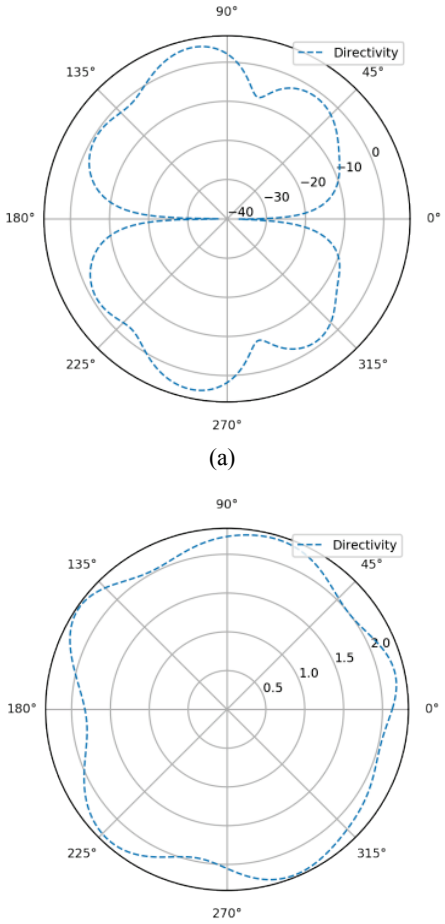

(a)

(b)

Fig. 9. Two dimensional radiation pattern of the antenna in (a) E-plane and (b) H-plane.

bandwidth BW can be defined as $BW = \frac{f_h - f_l}{f_{mn}} \times 100\%$. Here, f_l and f_h is the lower and the higher frequency of the bandwidth, respectively and f_{mn} is the resonant frequency in mn mode. It can also be observed that the bandwidth is significantly increased above −10 dB reflection coefficient. The reflection coefficient Γ_0 at load can be determined using $\Gamma_0 = \frac{z_l + z_0}{z_l - z_0}$. z_0 is the characteristic impedance and z_l is load impedance. The minimum value of voltage standing wave ratio ρ defined to be the ratio of the magnitude of the maximum voltage v_{max} to the magnitude of the minimum voltage v_{min} is achieved 1.01 at resonant frequency which is shown in Fig. 8. It may be formulated as $\rho = \frac{|v|_{max}}{|v|_{min}} = \frac{|v|_+ + |v|_-}{|v|_+ - |v|_-}$. It is noted that ρ is a measure of how well the input impedance matches with the load impedance. Once ρ is known, the reflection coefficient $|\Gamma|$ can be calculated by the equation $|\Gamma| = \frac{\rho - 1}{\rho + 1}$. The normalized complex load impedance of the antenna at resonant frequency is attained $49.7 + j0.18\ \Omega$. Hence, the load impedance z_l, being the complex conjugate of the input impedance z_i, has approximately matched the input impedance that is $z_l \approx z_i$

TABLE II
COMPARISON OF THIS WORK BASED ON FEW IMPORTANT FEATURES WITH RECENT RELATED WORKS

Ref.	Dimension (mm^3)	Operating bands (GHz)	Gain	Effic-iency
[31]	14×30×8	3.3/5.2/5.8	4.0dBi	80%
[32]	37×37×1.6	2.4/3.3/5.8	4.93dBi	NG
[33]	18×22×1.6	0.9/2.4/5.2	NG	NG
[34]	50×10×1	2.4/5.2	2.09dBi	NG
[35]	35×30×0.12	1.9/5.8	0.51dBi	55%
[36]	17.5×8×0.8	2.4/3.3/5.8	1.5dBi	80%
[37]	34×33×1.57	5	7dBi	95%
[38]	57×40×1.6	0.8/1.7/2.4/5	6.7dBi	NG
[39]	44×39×1.6	3.3/5/6.6/9.9	1.98dBi	78%
[40]	43×33×1.6	2.4/3.8/5	5.6dBi	NG
[41]	42×30×1.6	2.4/5	4dBi	90%
[42]	20×8.7×0.4	5/6	2.25dBi	80%
Pro-posed	$\pi\times(3.55)^2\times60$	6	4.37dB	89%

NG—Not Given

where $z_l = z_i^*$. It assures the maximum power transfer and minimum reflections from the load. The directivity D of the antenna defined as the ratio of its intensity of radiation u at a direction over the intensity of radiation u_0 from an isotropic source, on the other words, the ratio of the intensity of radiation in a direction to the intensity of radiation averaged over all directions is observed maximum 4.90 dB. It is expressed to be $D = \frac{u}{u_0}$. The two dimensional radiation pattern of the proposed antenna in the scenario of E and H planes with directivity is shown in Fig. 9. The radiation efficiency η_{rad} defined by the ratio of radiated energy E_{rad} to incident electrical energy E_{inc} is established at 89% from the proposed antenna and can be given as $\eta_{rad} = \frac{E_{rad}}{E_{inc}} \times 100\%$. It interprets that almost all the accepted electrical energy by the antenna will be dispersed as radiation into the surrounding area.

A comparison table including some important characteristics of an antenna is given in Table II.

VI. CONCLUSION

This paper presents a compact cylindrical shaped antenna that resonates at a frequency of 6.5 GHz for Wi−Fi applications in wireless routers. A material called FR4−Epoxy is utilized for the substrate layer of the antenna. The material has various useful properties, i.e. flexibility, compactness, shock resistivity, etc. It is also one of the most available materials throughout the world. Copper is used for the patch and the ground wire as it can easily be impersonated on any plane surface of the materials. The value of gain obtained 4.37 dB implies that the antenna is able to supply a strong network within a broaden hotspot properly. Radiation from the antenna become polarized circularly and overtakes the undesirable direction. It is an efficacious attribute of an antenna for Wi−Fi applications. The antenna achieved a value of 4.90 dB directivity. The lower reflection coefficient is obtained −49.5 dB. Voltage standing wave ratio meets a value of 1.01. More than 600 MHz or 9.2% wide bandwidth at −10 dB reflection coefficient covers the Wi−Fi 6 GHz frequency band (5.925−7.125) GHz. $49.7 + j0.18\ \Omega$ impedance determined reveals that it approximately matches input impedance. The remarkable radiation efficiency of 89% is observed from the proposed antenna.

REFERENCES

[1] Z. N. Chen, X. Qing, T. S. See, and W. K. Toh, "Antennas for Wi–Fi Connectivity", *Proceedings of the IEEE,* vol. 100, pp. 2322–2329, 8 March 2012.

[2] J. S. Lee, Y. W. Su, and C. C. Shen, "A Comparative Study of Wireless Protocols: Bluetooth, UWB, ZigBee, and Wi−Fi", *IECON 2007–33rd Annual Conference of the IEEE Industrial Electronics Society,* pp. 46–51, 5 November 2007.

[3] V. Talla, B. Kellogg, B. Ransford, S. Naderiparizi, S. Gollakota, and J. R. Smith, "Powering the Next Billion Devices with Wi−Fi", *Proceedings of the 11th ACM Conference on Emerging Networking Experiments and Technologies,* pp. 1–13, 1 December 2015.

[4] T. Pelkey, FCC Adopts New Rules for the 6 GHz Band Unleashing 1200 Megahertz of Spectrum for Unlicensed Use, Washington, 23 April 2020. Available: https://docs.fcc.gov/public/attachments/DOC-363945A1.pdf

[5] Z. Weng et al., "A 2.45GHz Microstrip Patch Antenna Evolved for Wi–Fi Application", *2015 IEEE Congress on Evolutionary Computation (CEC),* pp. 1191−1195, 25 May 2015.

[6] R. Roshan and R. K. Singh, "Dual ISM Band MIMO Antenna for Wi–Fi and WiMax Application", *2014 International Conference on Signal Propagation and Computer Technology (ICSPCT 2014)*, pp. 209–213, 12 July 2014.

[7] D. Chang and S. Yen, "High Gain Antenna Array with Finite Ground Plane for IEEE802.11a Wi–Fi Application", *IEEE iWEM2011*, pp. 125–129, 8 August 2011.

[8] M. S. R. Bashri, T. Arslan, and W. Zhou, "A Dual–Band Linear Phased Array Antenna for Wi–Fi and LTE Mobile Applications", *2015 Loughborough Antennas & Propagation Conference (LAPC),* pp. 1–5, 2 November 2015.

[9] J. F. Huang, and W. C. Lai, "Design of a Compact Printed Double–Sided Dual–Band Dipole Antenna by FDTD for Wi–Fi Application", *Microwave and Optical Technology Letters*, vol. 55, pp. 1845–1851, August 2013.

[10] B. Wu and Q. Feng, "A Broadband Antenna for Wi–Fi/WiMAX Application," *2016 IEEE International Workshop on Electromagnetics: Applications and Student Innovation Competition (iWEM)*, pp. 1–3, 16 May 2016.

[11] N. A. Malek, S. A. Karsin, S. Y. Mohamad, F. M. Isa, A. L. Asnawi, and A. M. Ramly, "Design of a Dual Band Printed Dipole Antenna for WI–FI Application", *Journal of Telecommunication, Electronic and Computer Engineering (JTEC),* vol. 9, pp. 63–68, 30 December 2017.

[12] S. Subahir, M. S. Amari, M. T. Ali, S. N. Kamarudin, and M. F. Jamlos, "Rectangular Spiral Microstrip Patch Antenna Integrated with LED for Wi–Fi Application", *2014 IEEE 2nd International Symposium on Telecommunication Technologies (ISTT),* pp. 76–79, 24 November 2014.

[13] A. Shafqat, and F. A. Tahir, "Miniaturized Tapered Meandered Dual Band Dipole Antenna for Wi–Fi 2.4/5.8 GHz Application", *2017 Progress in Electromagnetics Research Symposium – Fall (PIERS – FALL)*, pp. 1640–1642, 19 November 2017.

[14] A. Shafqat, F. A. Tahir, and M. U. Khan, "Textile Based Dual Band MIMO Quad−Mode Substrate Integrated Waveguide Antenna for Wi–Fi Application", *2017 Progress in Electromagnetics Research Symposium – Fall (PIERS – FALL),* pp. 1767–1770, 19 November 2017.

[15] M. E. de Cos, M. Mantash, A. C. Tarot, and F. Las–Heras, "Dual–Band Coplanar Waveguide–Fed Smiling Monopole Antenna for Wi–Fi and 4G Long–Term Evolution Applications", *IET Microwaves, Antennas & Propagation,* vol. 7, pp. 777–782, 18 June 2013.

[16] C. H. See, R. A. Abd–Alhameed, Z. Z. Abidin, N. J. McEwan, and P. S. Excell, "Wideband Printed MIMO/Diversity Monopole Antenna for Wi–Fi/WiMAX Applications", *IEEE Transactions on Antennas and Propagation,* vol. 60, pp. 2028–2035, April 2012.

[17] M. C. Derbal, A. Zeghdoud and M. Nedil, "A Novel Dual Band Antenna Design for Wi−Fi Applications Using Genetic Algorithms", *2018 IEEE International Symposium on Antennas and Propagation & USNC/URSI National Radio Science Meeting*, pp. 1009–1010, July 2018.

[18] H. T. Hsu, F. Y. Kuo, and P. H. Lu, "Design of Wi−Fi/WiMAX Dual−Band E−Shaped Patch Antennas Through Cavity Model Approach", *Microwave and Optical Technology Letters*, vol. 52, pp. 471–474, February 2010.

[19] A. A. Yassin, R. A. Saeed, and R. A. Mokhtar, "Dual−Band Microstrip Patch Antenna Design Using C−Slot for Wi−Fi and WiMax Applications", *2014 International Conference on Computer and Communication Engineering,* pp. 228−231, September 2014.

[20] R. Varma, J. Ghosh, and R. Bhattacharya, "A Compact Dual Frequency Double U–slot Rectangular Microstrip Patch Antenna for Wi−Fi/WiMAX", *Microwave and Optical Technology Letters,* vol. 59, pp. 2174–2179, September 2017.

[21] https://www.ansys.com/products/electronics/ansys-hfss

[22] K. M. Luk, K. F. Lee, and J. S. Dahele, "Input Impedance and Q Factors of Cylindrical Rectangular Micro Strip Patch Antennas", *IEEE Int. Conf. on Antennas and Propagation,* Part 1, pp. 95–98, June 1986.

[23] Y. T. Lo, D. Solomon, and W. F. Richards, "Theory and Experiment on Microstrip Antennas", *IEE Transactions on Antenna and Propagation,* vol. 27, pp. 137–145, March 1979.

[24] K. Carver and J. Mink, "Microstrip Antenna Technology", *IEEE Transactions on Antennas and Propagation*, vol. 29, pp. 2–4, January 1981.

[25] J. R. James, *Handbook of Microstrip Antennas*, IET, 1989.

[26] R. F. Harrington, *Time–Harmonic Electromagnetic Fields*, McGraw−Hill, 1961.

[27] J. Ashkenazy, S. Shtrikman, and D. Treves, "Electric Surface Current Model for the Analysis of Microstrip Antennas on Cylindrical Bodies", *IEEE Transactions on Antennas and Propagation,* vol. 33, pp. 295–300, March 1985.

[28] M. Kopp, *An Introduction to HFSS: Fundamental Principles, Concepts, and Use*, ANSYS, Inc., 275 Technology Drive, Canonsburg, PA 15317, USA, 2013.

[29] C. A. Balanis, *Antenna Theory: Analysis and Design*, John Wiley & Sons, December 2015.

[30] D. G. Fang, *Antenna Theory and Microstrip Antennas*, CRC Press, December 2017.

[31] Q. Guo, J. Zhang, J. Zhu, and D. Yan, "A Compact Multiband Dielectric Resonator Antenna for Wireless Communications", *Microw. Opt. Technol. Lett.*, vol. 62, pp. 2945–2952, September 2020.

[32] Y. Gong, S. Yang, B. Li, Y. Chen, F. Tong, and C. Yu, "Multi–Band and High Gain Antenna Using AMC Ground Characterized with Four Zero–Phases of Reflection Coefficient", *IEEE Access*, vol. 8, pp. 171457–171468, September 2020.

[33] P. Rajalakshmi and N. Gunavathi, "Compact Modified Hexagonal Spiral Resonator−Based Tri−Band Patch Antenna with Octagonal Slot for Wi−Fi/WLAN Applications", *Progress in Electromagnetics Research C*, vol. 106, pp. 77–87, 2020.

[34] Y. B. Yang, F. S. Zhang, Y. Q. Zhang, and X. P. Li, "Design and Analysis of a Novel Miniaturized Dual Band Omnidirectional antenna for Wi−Fi Applications", *Progress in Electromagnetics Research M*, vol. 94, pp. 95–103, 2020.

[35] A. Aziz, A. Motagaly, A. Ibrahim, W. Rouby, and M. Abdalla, "A Printed Expanded Graphite Paper Based Dual Band Antenna for Conformal Wireless Applications", *Int. J. Electron. Comm. (AEU)*, vol. 110, pp. 1–7, 1 October 2019.

[36] J. Kulkarni and C. Y.D. Sim, "Low−Profile, Compact Multi−Band Monopole Antenna for Futuristic Wireless Applications", *2020 IEEE International Conference on Electronics, Computing and Communication Technologies (CONECCT)*, pp. 1–5, 2 July 2020.

[37] A. Kumar, A. A. Althuwayb, and M. J. Al-Hasan, "Wideband Triple Resonance Patch Antenna for 5G Wi−Fi Spectrum", *Progress in Electromagnetics Research Letters*, vol. 93, pp. 89–97, 2020.

[38] N. Abbasi, R. Langley, and S. Bashir, "Multiband Shorted Monopole Antenna", *Journal of Electromagnetic Waves and Applications*, vol. 28, pp. 618–633, 24 March 2014.

[39] R. Saraswat and M. Kumar, "A Vertex−Fed Hexa−Band Frequency Reconfigurable Antenna for Wireless Applications", *Int. J. RF Microw. Comput. Aided Eng.*, vol. 29, pp. 1–13, October 2019.

[40] J. Jing, J. Pang, H. Lin, Z. Qui, and C. J. Liu, "A Multiband Compact Low−Profile Planar Antenna Based on Multiple Resonator Stubs", *Progress in Electromagnetics Research Letters*, vol. 94, pp. 1–7, 2020.

[41] Y. Kumar, R. Gangwar, and B. Kanaujia, "Asymmetrical Mirror Imaged Monopole Antenna with Modified Ground Structure for DBDP Radiations", *International Journal of Electronics*, vol. 107, pp. 1–24, 2 April 2020.

[42] J. Kulkarni and C.-Y.-D. Sim, "Wideband CPW−Fed Oval−Shaped Monopole Antenna for Wi−Fi 5 and Wi−Fi 6 Applications", *Progress in Electromagnetics Research C,* vol. 107, pp. 173–182, 2021.